









## Durability and mechanical properties of concretes with limestone filler with particle packing

 R.A. dos Santos<sup>a</sup> ,  G.R. Meira<sup>b</sup>,  W.M. Andrade Filho<sup>a</sup>,  M.C.B.M. Oliveira<sup>a</sup>,  V.K.S. Morais<sup>a</sup>,  
 S.F.F. Rodrigues<sup>a</sup>,  J.M. Neto<sup>a</sup>

a. Department of Civil Construction, Federal Institute of Education, Science and Technology of Paraíba, (Cajazeiras, Brazil)  
b. Department of Civil Construction, Federal Institute of Education, Science and Technology of Paraíba, (João Pessoa, Brazil)  
✉: [robson.santos@ifpb.edu.br](mailto:robson.santos@ifpb.edu.br)

Received 16 October 2023  
Accepted 08 April 2024  
Available on line 31 October 2024

**ABSTRACT:** This study aims to present alternatives to reduce the demand of cement in concrete production based on particle packing concepts. Physical and mechanical characteristics of concretes, as well as the resistance to chlorides action were analyzed. The tests conducted in this study included compressive strength, chloride migration, capillary absorption tests and wetting and drying cycles in 1M sodium chloride solution. Mixtures containing limestone filler presented satisfactory results compared to the reference mixture with particle packing. Excellent results were obtained for concrete with cement consumption of 253.34 kg.m<sup>-3</sup> in terms of compressive strength, binder index, capillary absorption and depassivation time of rebars, thus reinforcing the concept that partial cement replacement by limestone filler yields positive results in these properties. Worse results were obtained for concrete with a cement consumption of 161.86 kg.m<sup>-3</sup>, because it had a higher proportion of filler than cement. The electrochemical monitoring of the steel bars also shows that the packing of the aggregates was essential to delay the initiation of corrosion.

**KEY WORDS:** Chloride migration; Concrete durability; Packing; Sustainability.

**Citation/Citar como:** dos Santos RA, Meira GR, Andrade Filho WM, Oliveira MCBM, Morais VKS, Rodrigues SFF, Neto JM. 2024. Durability and mechanical properties of concretes with limestone filler with particle packing. Mater. Construcc. 74(355):e348. <https://doi.org/10.3989/mc.2024.366423>.

**RESUMEN:** *Durabilidad y propiedades mecánicas de los hormigones con filer calizo utilizando empaquetamiento de partículas.* Este estudio tiene el objetivo de presentar alternativas para reducir la demanda de cemento en la producción de hormigón teniendo en cuenta conceptos de empaquetamiento de partículas. y la resistencia a la acción de los cloruros fueron evaluados. Las pruebas realizadas en ese estudio fueron resistencia a la compresión axial, migración de cloruros, absorción capilar y ciclos de humectación y secado en solución de cloruro sódico 1M. Las mezclas que contienen filer calizo presentaron resultados satisfactorios en comparación con la mezcla de referencia con empaquetamiento de partículas. La mezcla con un consumo de cemento de 253,34 kg.m<sup>-3</sup> demostró excelentes resultados en términos de resistencia a la compresión axial, índice de aglomerante, absorción capilar y tiempo para despasivación del acero, reforzando el concepto de que la sustitución parcial del cemento por filer calizo produce resultados positivos en esas propiedades. Peores resultados fueron obtenidos para el hormigón con consumo de cemento de 161,86 kg.m<sup>-3</sup>, debido a su composición con mayor proporción de filer en comparación con el cemento. El monitoreo electroquímico de las barras de acero muestra que el empaquetamiento de los agregados fue esencial para el retardo de la iniciación de la corrosión.

**PALABRAS CLAVE:** Migración de cloruros; Durabilidad del hormigón; Empaquetamiento; Sostenibilidad.

## 1. INTRODUCTION

The construction industry faces constant challenges in the search for durable, economical, and sustainable building materials. In this context, concrete is one of the most widely used materials, both in small structures and in major infrastructure works. However, the need to improve concrete performance, especially in terms of durability and mechanical properties, has driven research aimed at optimizing these characteristics.

In developing countries, Portland cement plays a crucial role in infrastructure expansion and housing construction as it is widely used as a building material. Cement production is one of the main sources of greenhouse gas emissions; it is responsible for approximately 5%–8% of the global CO<sub>2</sub> emissions. Notably, cement production accounts for 95% of the total emissions related to concrete production (1). The demand for building materials, and consequently for cement, has grown globally. According to the Global Construction 2030 report produced by the consultancy Global Construction Perspectives and Oxford Economics, world cement production is estimated to increase from 4.2 billion tons in 2019 to 5.8 billion tons in 2030 (2). This increase in cement production can impose greater pressure on the environment and worsen air, soil, and water quality in the production regions.

In this context, it is important to seek more sustainable and efficient alternatives for cement. Some authors have pointed to the use of mineral additions as one of these alternatives. According to (3), mineral additions can improve the mechanical and thermal properties of concrete and reduce the demand for cement. The use of supplementary cementitious materials (SCMs) in the preparation of concrete can lead to significant energy and cost savings and environmental pollution reduction (4).

Limestone filler (LF) has been used in concrete and mortar for many years. In 1938, (5) first reported that CaCO<sub>3</sub> could react with cement to form calcium-carboaluminate. In 1977, (6) explain the formation of calciumcarboaluminate was influenced by the amount and fineness of LF, however, this formation apparently does not affect the compressive strength. According to a study by (7), up to 20% of the cement in concrete can be replaced by LF without drastically affecting the properties of the concrete.

LF contains particles of sizes smaller than 80 μm formed by the grinding of limestone rock. This material is usually considered an inert addition (8). It is added to concrete and mortar as a filling material, which increases the compactness and improves the particle size distribution of the concrete (7, 9).

In addition to high fineness, LF also has low chemical reactivity with cement, which can reduce the formation of undesirable compounds, such as ettringite (10). Substances such as ettringite can cause undesirable expansion and damage to the concrete structure. In addition, LF can reduce the permeability of concrete, thereby increasing its durability and resistance to aggressive agents (11).

In their review article, (12) discussed that although the use of LF to partially replace Portland cement will undoubtedly lead to environmental benefits, to be truly sustainable, the concrete with LF should have mechanical properties and durability equivalent to or superior than those achieved using regular Portland cement concrete. The lack of cementitious or pozzolanic properties of LF relative to SCMs is the predominant reason for limiting the substitution of Portland cement by LF. Therefore, it is important to encourage research that evaluates high LF loads and their implications on the durability of these concretes.

LF acts on cement-based materials through three mechanisms: the filler effect, nucleation, and chemical effect. The filler effect is strongly linked to the particle size. When the LF particles are finer than the cement grains, they fill in the empty spaces between the cement grains, improving the particle size distribution and, consequently, increasing their packing. Hence, greater compressive strength and material durability are achieved (13).

In the nucleation effect, the LF, which is a calcareous filler, serves as a center for the precipitation of hydration products, thereby accelerating hydration reactions (14–16). The energetic surface and adsorption ability of the calcareous filler increase with a reduction in its particle size (17). Hence, the calcareous filler tends to be more effective in forming hydrates than other mineral additions such as quartz or slag, and delivers a more pronounced nucleation effect than these admixtures (18).

The chemical effect of using LF in Portland cement originates from the formation of carboaluminates in the mixture. In general, inclusion of 4% of LF is sufficient to produce this effect. The chemical effect is influenced by the size of the LF particles, the amount of alumina in the cement, and other additives such as metakaolin. The calcareous filler can react with tricalcium aluminate or tetracalcium aluminoferrite in the cement or with aluminates from other mineral additions, thus forming carboaluminates. However, as the amount of aluminate phases in the clinker is limited, the chemical effect of the LF is normally moderate (18–21).

Addition of LF has been proven to be advantageous, especially in terms the improvement of workability, reduction of shrinkage, decrease in permeabil-

ity, and optimization of the mechanical properties of concrete (7, 9, 10, 22, 23).

The LF also plays an important role in sustainability because its use as a mineral addition allows reducing the amount of Portland cement needed in the mixture. Cement production is the major source of carbon dioxide (CO<sub>2</sub>) emissions. Thus, incorporation of LF will contribute to the reduction of CO<sub>2</sub> emissions associated with concrete production (24).

Particle packing is a promising approach for optimizing the compactness and efficiency of concrete. This technique fills the voids between the particles of aggregates, cement, and LF, yielding a denser and more homogeneous matrix. Studies have shown that particle packing helps to improve the durability and mechanical strength of concrete (25, 26).

Some studies, for example, that of Damineli (2013) propose the use of filler as a tool to increase the packing and dispersion of particles, improve the rheological behavior of the mixture and reduce the amount of water used in concrete and mortar.

To maximize the filler effect and obtain concretes with lower permeability, it is essential to perform a particle packing study. This study involves a careful analysis of the granulometric compositions of the materials using mathematical models, such as the modified Andreasen model (27). Based on the previous granulometry analyses, an attempt is made to fill the spaces between the larger grains with smaller particles based on calculations or experiments. The aim was to achieve the maximum compaction among the particles of the composite material to reach improved compressive strength, greater durability, and extension of the service life of structural components.

In this work, Portland cement was replaced by LF in concretes, and the response of the mechanical properties and corrosion resistance of steel embedded in these concretes were verified in chloride cycles.

In this study, components were carefully selected using a specialized software called Q-mix. This software uses particle packing algorithms to optimize the formulation of materials and was developed as part of a doctoral thesis by the first author of this work. The purpose of this software is to provide a precise mathematical approach to maximize the compactness and efficiency of the materials.

The use of the Q-mix software is justified by its capacity to simulate and optimize the disposition of the

particles in concrete, considering different factors such as the characteristics of the aggregates, proportion of LF, and granulometric distribution of cement. Using mathematical models, Q-mix can determine the best combination of components to achieve a dense and homogeneous concrete matrix, thus providing a material with better mechanical properties and greater durability (28).

This study aimed to analyze the influence of particle packing on the mechanical properties and durability of concrete with low cement consumption and high levels of LF.

## 2. MATERIALS AND METHODS

Concrete was prepared using fine and coarse aggregates, binders, mineral addition, chemical admixtures, and water. Sand, which was used as a fine aggregate, was classified into three granulometric ranges: fine sand, medium sand, and coarse sand. The coarse aggregate was a granitic crushed rock gravel. A high-early strength Portland cement was used as the binder and LF as mineral addition. The used chemical admixture was a polycarboxylate-based superplasticizer, which allowed to obtain a concrete with a low water/cement ratio and an suitable level of workability. Finally, the used water was from the public water supplier of the Paraíba state in Brazil.

### 2.1. Cement

The high-early strength Portland cement used followed the specifications from the Brazilian standard (29). This cement does not have any pozzolanic addition, and thus, the influence of this kind of mineral addition could be neglected. Table 1 summarizes the chemical composition of the cement used, obtained from X-ray fluorescence (FRX) test.

The specific mass of the cement was determined to be 3.04 g/cm<sup>3</sup>, according to Brazilian standard (30). In addition, a laser granulometry test was conducted on the material using laser diffraction in a CILAS 1090 SECO equipment, which can measure particles within a range of 0.10–500.00 μm, based on the theories of Mie and Fraunhofer, which is divided into 100 classes. The results of the granulometric analysis of the cement can be seen in Figure 1.

TABLE 1. Chemical composition of the cement used.

Oxides	SiO <sub>2</sub>	Al <sub>2</sub> O <sub>3</sub>	Fe <sub>2</sub> O <sub>3</sub>	MgO	K <sub>2</sub> O	Na <sub>2</sub> O	TiO <sub>2</sub>	CaO	BaO	P <sub>2</sub> O <sub>5</sub>	SO <sub>3</sub>	MnO	LoI
(%)	22.11	3.99	3.41	1.97	0.6	0.3	0.37	62.25	0.09	0.64	3.51	0.03	6.80

LoI – Loss on ignition

### 2.2. Limestone filler

Limestone filler granulometry was performed using the same test and equipment described in section 2.1. From this test, the average size of the filler particles was 14.90  $\mu\text{m}$ , as shown in Figure 2. Notably, the fineness of the filler was close to that of Portland cement, suggesting the possibility of partially replacing the binder by LF, as proposed by (31) based on previous tests.

In addition, the chemical composition of the filler was determined through an X-ray fluorescence (FRX) test. The FRX results are summarized in Table 2.

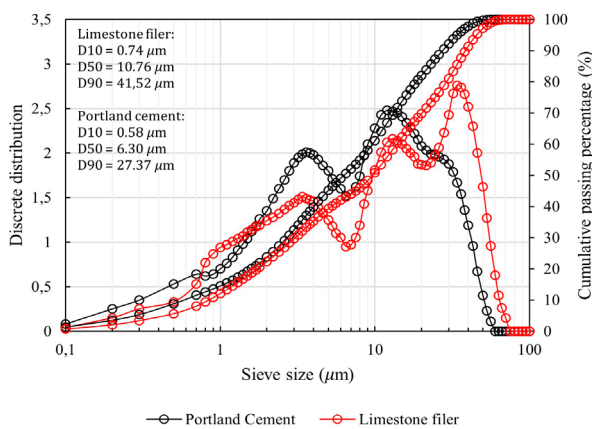


FIGURE 1. Laser granulometry of Portland cement and limestone filler. D10, D50 and D90 are the mesh sizes of the sieve through which 10%, 50% and 90% of the sample passes, respectively.

### 2.3. Aggregates

For an appropriate packing, it is desirable to sort aggregates based on their granulometric characteristics. In the present case sand was sorted and classified as fine, medium, and coarse sand. This sorting was achieved by sieving the sand through different meshes of sieves. To separate the coarse sand, a 1.2 mm sieve was chosen. Then, medium and fine sands were separated using a 0.6 mm sieve mesh.

As a result, sand 1 (coarse sand) comprises the fraction of the sand retained in the 1.2 mm sieve, and the sand that passed through the 1.2 mm sieve and was retained in the 0.6 mm sieve was designated as sand 2 (medium sand). Finally, the sand that passed through the 0.6 mm sieve was designated as sand 3

(fine sand). To determine the granulometric composition of each sand, the specifications of the Brazilian standard (32) were followed. Two different granite gravels were used in this work, gravel 0 (9.5 mm) and gravel 1 (19 mm).

The specific masses of the sands were obtained according to the Brazilian standard (33).

Regarding that aggregates characterization is essential to achieve the particle packing objective, Figure 2 shows the granulometric curves of the different aggregates used in concrete mixtures.

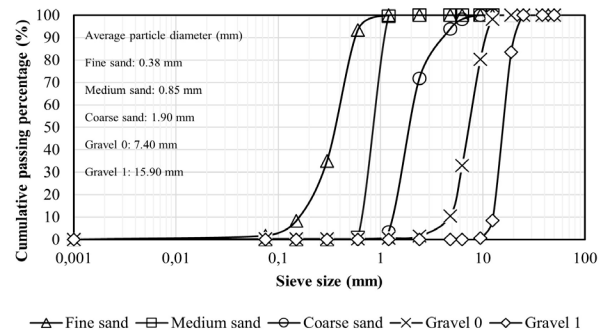


FIGURE 2. Aggregate granulometric curves.

Furthermore, Table 3 shows the specific masses of the used aggregates, which values with the granulometric distributions are helpful to build the concrete mixtures based on packing principles.

TABLE 3. Specific masses of the aggregates.

Specific mass (g/cm <sup>3</sup> )				
Fine sand	Medium sand	Coarse sand	Gravel 0	Gravel 1
2.66	2.64	2.65	2.63	2.64

### 2.4. Concrete mixtures

#### 2.4.1 Particle packing

To reach the appropriate particle size distribution and meet the packing condition, the modified A&A model (or Alfred) theoretical model was used. The virtual granulometric distribution should be approximately equal to the real system, as proven via numerical simulations and using real mixtures by (28).

TABLE 2. Chemical composition of the limestone filler.

Oxides	CaO	SiO <sub>2</sub>	Fe <sub>2</sub> O <sub>3</sub>	K <sub>2</sub> O	SrO	CuO	MnO	LoI
(%)	95.743	3.455	0.46	0.101	0.1	0.09	0.05	37.08

To reach the suitable choice of the fraction of each aggregate, regarding the appropriate diameters of the particulate materials and the principle that the larger voids should be filled by the smaller particles, the Q-Mix software was developed by (28). The software contributes to the calculation of the optimal proportion of each aggregate fraction, optimizes the mixture of aggregates, and improves understanding the modified Andreasen packing model.

For a better comprehension, a step-by-step instruction for using Q-Mix to optimize packaging is presented.

*Step 1:* Feeding data obtained in the aggregate granulometry tests.

The user is asked to enter the data obtained through the granulometry test and name the respective aggregates.

*Step 2:* Selection of the input parameters.

To calculate the ideal granulometric curves using packing models, the software adopts modified A&A model; the user can select the minimum diameter ( $D_s$ ), the maximum diameter ( $D_L$ ), and distribution module ( $q$ ) to be used.

The input data were the distribution modulus “ $q$ ”, the largest and the smallest aggregate diameter ( $D_L$  and  $D_s$ , respectively).  $D_L$  and  $D_s$  values were fixed at 9.5 mm (gravel 9.5mm) and 0.075 mm (fine sand), respectively, which were obtained from the granulometric analysis of the aggregates in Q-Mix.

The optimization algorithm was developed through the linear programming, a mathematical modeling technique in which a linear function is maximized or minimized when subjected to various constraints. Using the individual granulometric curves (PSD) of each aggregate, the simulations (Q-Mix) calculated the optimal aggregate percentages required to plot a numerical PSD curve (mixture) with minimum deviation to its respective mathematical PSD curve (Modified A&A model).

In Table 4 it is presented the mathematical solution to the case of a mixture with “ $m$ ” aggregates and “ $n$ ” sieves/particle size classes.

Where:

$\Phi_i$  – Sieve/particle size class “ $i$ ”;  
 $pe_i$  – Accumulated retained percentage in sieve “ $i$ ”, calculated by the modified A&A model;

$pa_{j,i}$  – Accumulated retained percentage in sieve “ $i$ ” for aggregate  $a_j$ ;

$pc_i$  – Accumulated retained percentage in sieve “ $i$ ” for the combination of aggregates 1, 2, ...,  $m$ ;

$\Delta_i$  – Deviation between the accumulated percentage of aggregates retained in sieve “ $i$ ” and its respective recommended accumulated retained percentage by the mathematical model;

RSS – Deviation between the numerical PSD and the mathematical PSD, calculated as a residual sum of squares, where:  $i$  varies from 1 to  $n$ , and  $j$  varies from 1 to  $m$ .

The packing optimization is performed through linear programming, in which the objective function to be minimized corresponds to the RSS (1), and the imposed restriction is  $\sum_1^m \beta_j = 100\%$ . Therefore, the optimization consists in varying the coefficients  $\beta_j$  until a minimum RSS value is found.

$$RSS = \sum_1^n \Delta_i^2 = \frac{(pc_i - pe_i)^2}{100} \quad [1]$$

Where:

$$pe_i = \frac{D_i^q - D_s^q}{D_L^q - D_s^q} \times 100 \text{ (Modified A\&A model)}$$

$$pc_i = \sum_j^m \beta_j pa_{j,i}$$

*Step 3:* Run the software the mixture and obtain the optimized percentages.

After selecting the input parameters and running the algorithm, the modified A&A model will appear in the lower left corner of the screen. At this moment, the “solve” command must be clicked on.

TABLE 4. Calculation process of the deviation (RSS) between the numerical and the mathematical PSD curves for a mixture with  $m$  aggregates.

$\Phi$	$pe(\%)$	$pa_1(\%)$	$pa_2(\%)$	...	$pa_m(\%)$	$pc(\%)$	$\Delta$
$\Phi_1$	$pe_1$	$pa_{1,1}$	$pa_{2,1}$	...	$pa_{m,1}$	$pc_1$	$\Delta_1 = pc_1 - pe_1$
$\Phi_2$	$pe_2$	$pa_{1,2}$	$pa_{2,2}$	...	$pa_{m,2}$	$pc_2$	$\Delta_2 = pc_2 - pe_2$
...	...	...	...	...	...	...	...
$\Phi_n$	$pe_n$	$pa_{1,n}$	$pa_{2,n}$	...	$pa_{m,n}$	$pc_n$	$\Delta_n = pc_n - pe_n$
RSS							$\sum \Delta_i^2$



FIGURE 3. Example of packing calculation for three chemical a content of aggregates in Q-Mix.

To obtain more satisfactory results, the chosen aggregates must be of good quality, as the calculation of the software is based on the input data.

Figure 3 shows the Q-mix software screen, in which a random example is presented with data of three aggregates from the local commerce (Cajazeiras-PB/Brazil).

### 2.5. Preparation, curing, and casting of the test specimens

Initially, all the materials necessary for preparing concrete were separated and temporarily stored. The materials included the Portland cement; limestone filler; fine, medium and coarse sand; small gravel; superplasticizer and water. The dry materials were

stored in translucent plastic bags, and the superplasticizer and water were stored in beakers and buckets.

Table 5 summarizes the information on the consumption of materials used in concrete mixtures. The informed data correspond to an aggregate optimization process to determine the ideal percentage to ensure the best performance of these materials. The water/fines ratio was maintained at 0.44 for concretes with packaging, except for T160 concrete, which, due to the higher content of LF, required a greater amount of water for the desired slump of about 120mm.

The aggregate contents were calculated using Q-mix software (28), which allows to determine the ideal proportion of materials considering the previously informed data.

Regarding admixtures, 1.8% of the total mass (cement) was used in the concretes with filler, except for

TABLE 5. Concrete mixtures.

Concrete	Consumption of concrete materials (kg/m <sup>3</sup> )									
	Cement	Limestone filler	Fine sand	Medium sand	Coarse sand	Gravel 0 (9.5 mm)	Gravel 1 (19 mm)	Water	Water/fines	Slump (mm)
T160	161.86	222.56	200.70	437.83	510.66	674.95	–	178.05	0.46	120
T240	253.34	129.78	203.92	443.14	517.83	685.58	–	170.12	0.44	120
T320	327.13	61.34	202.82	442.44	516.05	683.06	–	172.42	0.44	125
T – RCE	384.00	–	203.13	447.51	519.53	687.44	–	170.25	0.44	130
T – RSE	384.01	–	–	874.03	–	–	978.05	170.62	0.44	125

concrete T160, which required 2.2% of superplasticizer. For reference concrete (T-RCE and T-RSE) 0.8% of superplasticizer was used.

The concrete preparation procedure started with the introduction of gravel and some amount of water in a 150 l concrete mixer. A few seconds after the equipment turned on, a half of the binder was added, followed by the intercalated pouring of all of the coarse sand to promote better mixing with the binder, especially in filler mixes. Then, most of the water was added to the mixer, leaving only a small amount in the bucket to mix with the chemical admixture if necessary. Then, medium and fine sand were added gradually. A few seconds after the mixture started rotating in the mixer, the rest of the binder was added. Finally, the additive was added to the concrete along with the remained water calculated and stored in the beakers.

The concrete was cast into cylindrical metal molds (dimensions: 10 × 20 cm). For each concrete mixture, 12 specimens were cast, which were mechanically compacted. After 24 h of cast, the specimens were demolded, identified, and submerged in a saturated lime water solution (25 ± 2°C) for 7 and 28 days to perform compressive strength tests.

## 2.6. Destructive and nondestructive tests

### 2.6.1. Compressive strength test

Axial compressive strength tests were carried out at 7, 28, and 90 days on cylindrical specimens, following the Brazilian standard (34). For these tests, a hydraulic press, which is located in the IFPB Structures Laboratory, Campus Cajazeiras, was used.

### 2.6.2. Chloride migration test

These tests were conducted according to the guidelines established in the procedure for specimen preparation and the migration test described in (35). This

standard determines the migration coefficient of chlorides in concrete, mortar, and other cement-based material using a non-steady-state migration method. This coefficient is used as an indicator of the resistance of the material to chloride penetration.

After a period of curing in a tank containing saturated lime solution, two cylindrical samples (dimensions: 10 × 20 cm), aged 28 days, for each concrete mixture (T160, T240, T320, T-RSE and T-RCE) were removed from the tank. The specimens were divided into five parts: they were cut perpendicular to their longitudinal axis, and the extremities were discarded, while the remaining three parts were used in the migration test. Thus, for each specimen, three samples were selected, and thus, six samples were tested for each concrete mixture.

Before starting the test, the specimens were water-proofed in the entire lateral surfaces and saturated in lime water solution under vacuum. Then, the specimens were packed in PVC tubes to ensure that only the circular surface faces were in contact with the solutions.

Two different solutions, one cathodic and the other anodic, were prepared. The cathodic solution was stored in an acrylic container and contained 100 g of NaCl for every 900 g of water. This solution was connected to the negative pole of the power supply using a stainless steel electrode. The anodic solution contained 12 g of NaOH for each liter of water and was placed in a plastic tube above the samples. This solution was connected to the positive pole of the power supply also using a stainless steel electrode. Both solutions were maintained within a specific temperature range, usually 20°C–25°C. Figure 4 shows all the details of the NT Build test (35).

During the test, the specimens were subjected to a potential difference between the cathodic and anodic solutions. The test results were used to evaluate the resistance of concrete to the chloride migration.

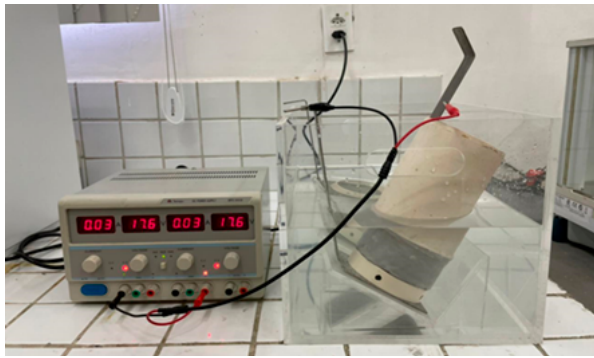


FIGURE 4. Assembly of the migration test set.

After the testing period, specimens were splitted into two parts with a thickness of 50 mm. Then, a colorimetric indicator solution was sprayed. In this case, the concrete surface was brought into contact with a  $\text{AgNO}_3$  solution, thereby initiating a chemical reaction that resulted in the formation of a white precipitate containing free chloride ions. Thus, the penetration of chlorides into concrete was measured. Afterwards, the migration coefficient was calculated according to NT Build test (35) recommendations.

### 2.6.3. Capillary absorption test

Capillary absorption tests were performed to evaluate the capacity of concretes to absorb water through its capillary pores. This test is important because excessive water absorption in concrete can have deteriorating effects, such as corrosion of reinforcements, decrease in mechanical strength, and formation of cracks. That is, capillary absorption tests provide important information about the water absorption capacity of a material, thereby helping to identify possible durability problems and boosting the development of concrete protection and conservation strategies.



The capillary absorption test process followed the guidelines described in the Brazilian standard (36). The specimens were stored in water saturated lime solution and were removed from the solution after 56 days for testing. These specimens were then placed in an oven at  $105^\circ\text{C} \pm 5^\circ\text{C}$  until reaching a constant mass. The samples were kept in the oven until the difference between two consecutive weighing, conducted at intervals of 24 h, did not exceed 0.5% of the obtained value. When this equilibrium was reached, the specimens were cooled to  $23^\circ\text{C} \pm 2^\circ\text{C}$ , and their masses were determined again.

In the test, the specimens were placed on a support at the bottom to ensure that they did not come into contact with the container. Conductor wires with cross sections of  $1.5\text{mm}^2$  were used so that the amount of water remained constant, as it was maintained up to a height of  $5 \pm 1$  mm above the lower face of the specimens. The container was then maintained at room temperature ( $25 \pm 2^\circ\text{C}$ ).

During the test, the mass of the specimens was measured at intervals of 3, 6, 24, 48, and 72 h from the moment that they were placed in contact with water. Before each measurement, the specimens were dried with a cloth. After the last weighing, the specimens were longitudinally splitted in two parts, as recommended by Brazilian standard (37), to enable the analysis of the water distribution inside them.

Calculations to determine the absorption coefficient (C) were performed using an Excel spreadsheet. The coefficient C was obtained by dividing the saturated mass minus the dry mass by the cross-section area.

### 2.6.4. Wetting and drying cycles in NaCl solution

The test consists of subjecting the specimens to wetting and drying cycles in aggressive solution. The wetting semi-cycle was characterized by a total im-



FIGURE 5. Wetting and drying test setup.



mersion in a 1M sodium chloride solution for 2 days and the drying semi-cycles was performed in an oven at 40°C for 5 days (Figure 5). The adopted solution had a concentration commonly reported in the literature (38-40) and the characteristics of the drying period was similar to some previous works (39, 41).

2.6.5. Electrochemical monitoring

Electrochemical monitoring was conducted by measuring the corrosion potential in an open circuit setup and the polarization resistance (Rp) with ohmic drop compensation, which was used to obtain the instantaneous corrosion current density. This technique is widely used in studies on the critical content of chlorides to detect depassivation of reinforcement (42-44).

The equipment used in the electrochemical measurements was a bench potentiostat, model VersaSTAT 3, Princeton Applied Research. A Cu|CuSO<sub>4</sub> (ESC) reference electrode and a stainless-steel counter electrode were used, and following the methodology used by (45). All the measurements were carried out in a Faraday’s cage to avoid any external interference.

The American standard (46) suggests the probability of corrosion based on the measured corrosion potential (Table 6).

TABLE 6. Classification of corrosion potentials according to (46).

Potential - E (mV -ESC)	Corrosion probability
E > -200	<10%
-200 ≥ E ≥ -350	Uncertainty about corrosion
E < -350	>90%

The Rp technique assume that there is a linear relationship between a small polarization ( $\Delta E < 20$  mV) around the open-circuit corrosion potential and the corresponding current ( $\Delta I$ ) variation, such that  $R_p = \Delta E / \Delta I$ , where  $R_p$  is the polarization resistance. Once  $R_p$  is determined, the reinforcement corrosion current density in concrete,  $I_{corr}$ , can be estimated using the Stern–Geary Equation [2] (47):

$$I_{corr} = \frac{\beta_a \times \beta_c}{2,3(\beta_a e \beta_c) \times \frac{\Delta I}{\Delta E}} \quad [2]$$

As  $R_p = \frac{\Delta E}{\Delta I}$  and  $B = \frac{\beta_a \times \beta_c}{2,3(\beta_a e \beta_c)}$  the

Equation can be simplified as follows:

$$I_{corr} = \frac{B}{R_p} \quad [3]$$

where:

$\beta_a e \beta_c$  = anodic and cathodic Tafel constants, respectively;

$\Delta E$  = applied potential;

$\Delta I$  = current variation;

B = Stern–Geary constant.

Tafel constants can be determined experimentally, but a high polarization is necessary for this measurement. High polarization will cause irreversible disturbances in the system. Therefore, using Equation [3], B = 26 mV is adopted (48), considering the reinforcement inserted in the concrete under an active condition.

Dividing the value of  $I_{corr}$  by the exposed area to corrosion, the corrosion rate per unit area is obtained, and it is normally expressed in units of microamperes per square centimeter. Values of  $i_{corr}$  below 0.1  $\mu A/cm^2$  indicate negligible corrosion from a practical

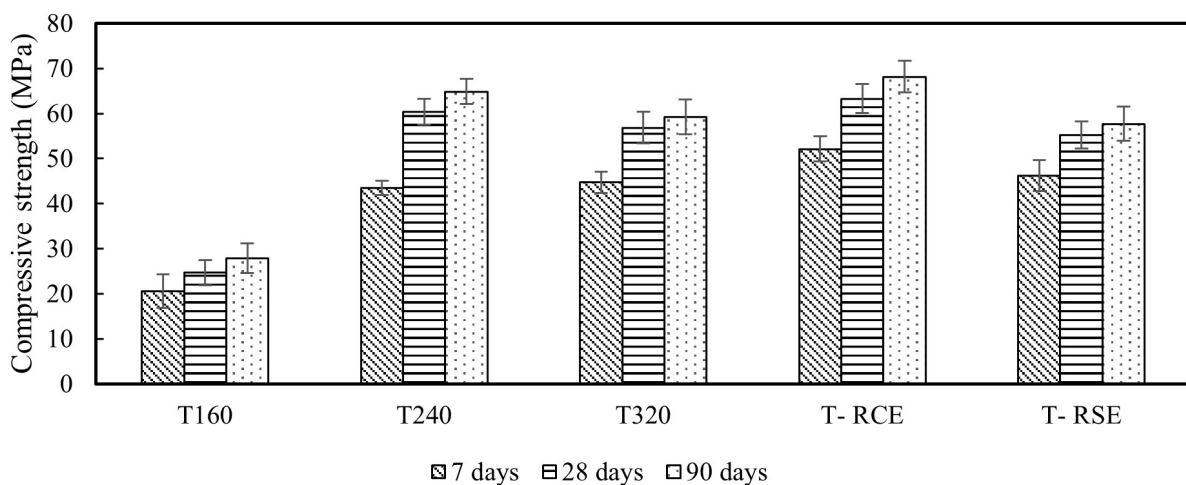


FIGURE 6. Compressive strength of the studied concretes at 7, 28, and 90 days.

point of view, and therefore, the steel reinforcement can be classified as “passive” (48).

### 2.7. Statistical analysis

The data experimentally obtained were analyzed using the statistical tool analysis of variance. This tool allows one to compare multiple groups, based on the F test, to establish the acceptance or rejection of the null hypothesis (Ho), which is determined through equality between the compared means. In addition, the Tukey test was performed for the data characterization process to identify differences and homogeneity of variance between groups. The significance level adopted for the study was 5%.

## 3. RESULTS AND DISCUSSION

### 3.1. Compression Strength

Figure 6 presents the results of the axial compressive strength tests for each mixture. It can be seen the effect of an increasing percentage of LF mass on the compressive strength at 7, 28, and 90 days.

As expected, it was verified that the compressive strength increased with time and decreased with the addition of LF, except for the T240 concrete, which presents an intermediate LF content. When comparing the other mixtures containing filler with the T240 concrete, which exhibited the highest compressive strength at all ages and had a better performance than the reference mixture without packing at the ages of 28 and 90 days. It is important to emphasize that the mixtures T160, T240, T320, T-RCE, and T-RSE reached the minimum compressive strength of 20 MPa at 28 days, as required by the Brazilian standards.

(49) concluded that, in some replacement ranges, the addition of LF caused an increase in the compressive strength of the concrete, whereas in other proportions, there was a decrease in this property.

Other studies also corroborate this trend of a reduction in compressive strength with an increase in the LF content in concrete. For example, (9) reported a decrease in compressive strength with an increase in LF content in concrete. The authors concluded that increasing the LF content reduced the compressive strength because LF was less reactive than Portland cement.

The influence of LF content on compressive strength of concretes is more significant at higher replacement levels because, at lower levels, the packing of the cementitious matrix promoted by the filler compensates the reduction of cement hydration products (50). Replacing part of the cement by LF increases the effective water to binder products and provides more space for hydration products, increasing the hydration degree of the binders. In addition, the filling effect and the heterogeneous nucleation of LF also contribute to the compressive strength increase. As a result, when small proportions of Portland cement are replaced by LF, there may be an increase in compressive strength (23). Figure 7 presents the results of the statistical analysis of the compressive strength results.

The results of the Tukey test showed a statistically significant difference in the compressive strength of the T-160 mix compared with all the other analyzed mixes (T-240, T-320, T-RCE, and T-RSE), indicating that T-160 has a different and lower compressive strength. Another important analysis was the comparison of the T-240 concrete with the other concretes; T-240 did not show any statistically significant difference to the T320 concrete, even though the latter contained 29.12% more Portland cement. This result indicates that this filler replacement proportion achieved the best matrix packing.

### 3.2. Binder intensity

Obtaining concrete with low environmental impact comprises much more than only replacing clinker by mineral additions. To produce more environmentally efficient concretes, it is necessary to reduce the binder consumption while increasing or maintaining the mechanical performance. Based on this premise, (51) proposed an indicator called binder intensity (Bi), which evaluates the efficiency of concrete considering the amount of binder needed to reach a mechanical strength of 1 MPa. Thus, the Bi allows a more comprehensive analysis of the efficiency of concrete, considering both the environmental aspect and the mechanical performance.

$$Bi = \frac{C}{R} \quad [4]$$

where,

	T160	T240	T320	T-RCE
T160				
T240				
T320				
T-RCE				
T-RSE				
Shows statistical difference		No statistical difference		

FIGURE 7. Tukey test for compressive strength of concrete.

**TABLE 7.** Compressive strength and Binder Intensity of studied concretes at 7, 28 and 90 days

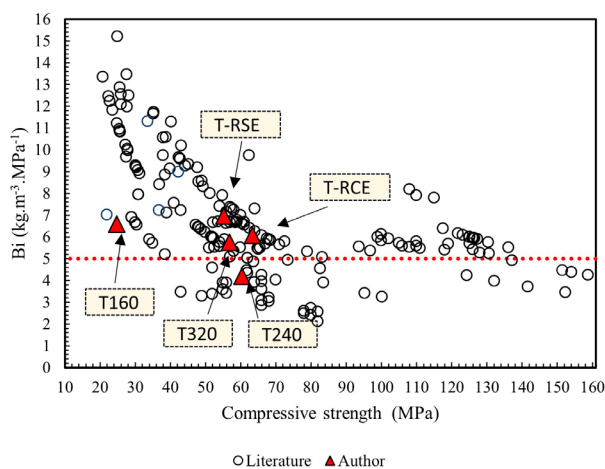
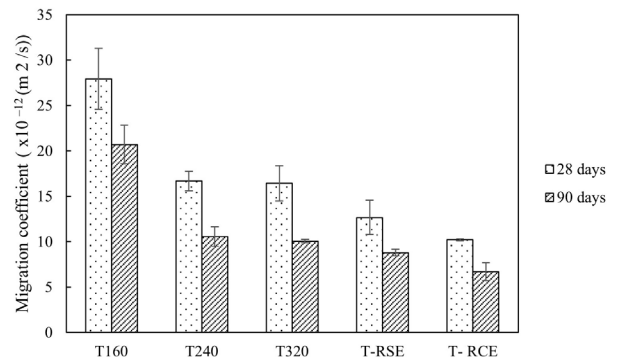
Concrete	Cement consumption (kg/m <sup>3</sup> )	Binder intensity					
		Compressive strength (MPa)			<i>Bi</i> - 7 days	<i>Bi</i> - 28 days	<i>Bi</i> - 90 days
		7 days	28 days	90 days			
T-160	162.65	20.59	24.71	27.94	7.90	6.58	5.82
T-240	253.33	43.51	60.40	64.87	5.82	4.19	3.90
T-320	327.13	44.72	56.84	59.26	7.32	5.76	5.52
T - RCE	384.01	52.14	63.30	68.12	7.74	6.07	5.63
T - RSE	384.00	46.16	55.18	57.72	8.32	6.96	6.65

$Bi$  = binder intensity, in  $\text{kgm}^{-3} \text{MPa}^{-1}$ ;  
 $C$  = cement consumption ( $\text{kgm}^{-3}$ );  
 $R$  = compressive strength (MPa).

For each concrete mixture analyzed, the Binder Index ( $Bi$ ) was calculated considering the compressive strength at 7, 28, and 90 days, along with the respective cement consumption. Following the classification proposed by (52), which considers high-efficiency concretes as those with an  $Bi$  of up to  $5 \text{ kgm}^{-3} \text{MPa}^{-1}$ , at 28 days, the obtained values were compared to determine the efficiency of the studied concretes. Table 7 presents all the  $Bi$  results for all concrete mixtures.

From the data in Table 7, it can be seen, in general, that the  $Bi$  decreases as the LF content increases. In the particular case of T240 concrete,  $Bi$  assumed the lowest values, showing that an optimal percentage of cement replacement by filler can be reached to concrete achieve a good binder index. This result shows that T240 concrete presented a better performance than the reference concrete using packing procedures.

Figure 8 shows the  $Bi$  results extracted from the literature and the concrete results of this study (9, 31, 53-63). It can be observed that the studied con-


**FIGURE 8.** Relationship between binder intensity and compressive strength at 28-days - literature and experimental data.

**FIGURE 9.** Migration coefficients for the studied concretes.

cretes present good results compared to other works that studied different concretes with different types of mineral additions.

### 3.3. Chloride migration

Non-steady-state accelerated migration tests were performed at 28 and 90 days of age for the studied concretes, following the procedures described by (35). The migration coefficient values obtained for each experimental condition at their respective ages are shown in Figure 9.

The results showed that the partial replacement of Portland cement by LF increased the chloride migration coefficients ions at all ages compared to the reference mixtures.

Furthermore, there was a significant reduction in the migration coefficients in concretes with advanced curing ages. For example, concrete T160 was 25.92% more resistant to chloride ingress at 90 days than at 28 days of curing. In the mixtures with higher cement contents, chloride migration coefficient decreased, but the reduction was less significant than that observed in the first test at 28 days.

The results obtained in this work are in agreement with the results reported by (23). These authors argued that chloride penetration into concrete were deeper in concretes containing LF than in concretes that did not have this kind of mineral addition. These authors explain that the deeper penetration of chloride ions in these concretes are related to the higher level of OH<sup>-</sup> ions present in the pore fluid of the concrete made with LF, and the characteristics of the porous and connected paste–aggregate interfacial transition zone (ITZ) associated with LF particles addition. (64) suggested that the OH<sup>-</sup> ions present in the pore fluid act as a supporting electrolyte and are responsible for the transportation of a significant amount of charge during chloride ion permeability test because of its

**TABLE 8.** Classification according to the penetration resistance of chlorides (66).

Chloride migration coefficient ( $D_{28} \times 10^{-12} \text{ m}^2/\text{s}$ )	Resistance to chloride penetration
>15	Low
10–15	Moderate
5–10	High
2.5–5	Very high
<2.5	Extremely high

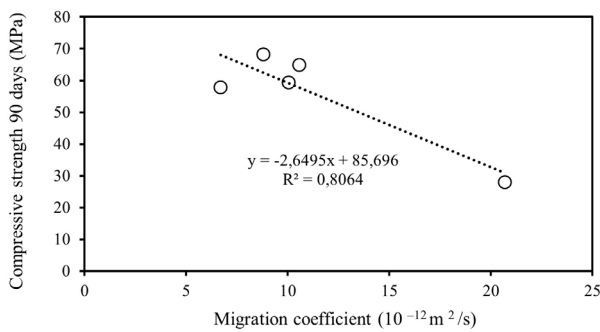


**FIGURE 10.** Correlation between chloride migration coefficients and compressive strength.

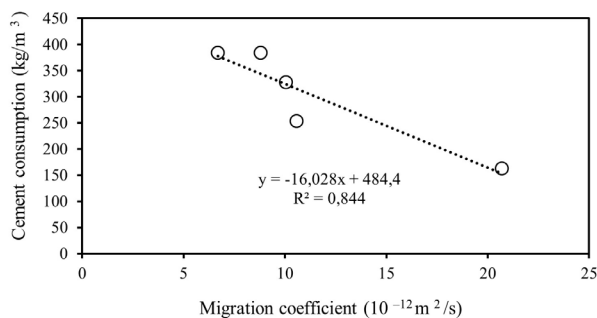


**FIGURE 11.** Correlation between chloride migration coefficients and cement content.

higher ionic conductivity than the other ions present in pore fluid (Na<sup>+</sup>, K<sup>+</sup> and Ca<sup>2+</sup>). (65) reported a reduction in chloride migration coefficients when a blast furnace and LF were used. However, they used much less LF than that used in this research.

Considering the classification presented in Table 8, T-RCE and T-RSE concretes demonstrated moderate resistance to chloride migration, whereas the T-320, T-240, and T-160 concretes showed low resistance at 28 days.

Chloride migration coefficients were correlated with other concrete study parameters, such as compressive strength and cement consumption. The results obtained are presented in Figures 10 and 11.

When comparing the results of chloride migration coefficients with the compressive strength and cement content, it was observed that cement content correlates better with migration coefficients. However, chloride migration coefficient also presents good correlation with compressive strength ( $R^2 = 0.8064$ ).

(67) stated that compressive strength is directly related to concrete durability, including the reduction of the chloride migration coefficient. They explained that a denser and more resistant concrete matrix is less porous, which makes it difficult for chloride ions to penetrate.

By analogy, the graph in Figure 11, which correlates cement content to the chloride migration coefficient, also reinforces the conclusion that the greater the cement content, the less easy it is for chlorides to penetrate into the concrete, which presents relation with the increasing chloride binding ability of concretes with higher cement content.

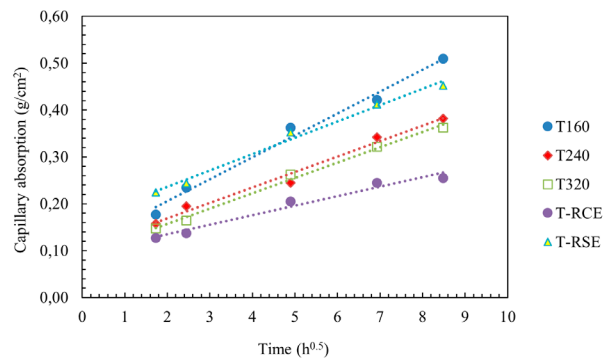


**FIGURE 12.** Correlation between capillary absorption and square root of time.

### 3.4. Capillary absorption

Water capillary absorption by the capillarity of cylindrical specimens (C) is calculated using the following Equation:

$$C = \frac{Msat - Ms}{s} \quad [5]$$

Where Msat (g) is the saturated mass of specimen, Ms (g) is the mass of the dry specimen and S is the cross-section area (cm<sup>2</sup>).

When plotting a graph with the values of C (g.cm<sup>-2</sup>) against the square root of time, a linear relationship is observed, as shown in Figure 12. The slope of this curve is the coefficient of capillary absorption.

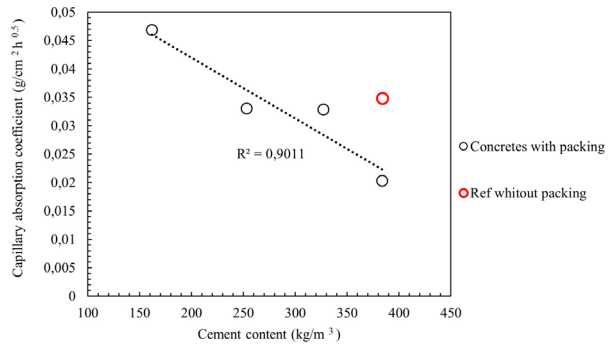


FIGURE 13. Correlation between capillary absorption coefficient and cement content.

The mixtures containing an adequate proportion of LF resulted in good absorption results. However, the T160 concrete, which contains a high amount of

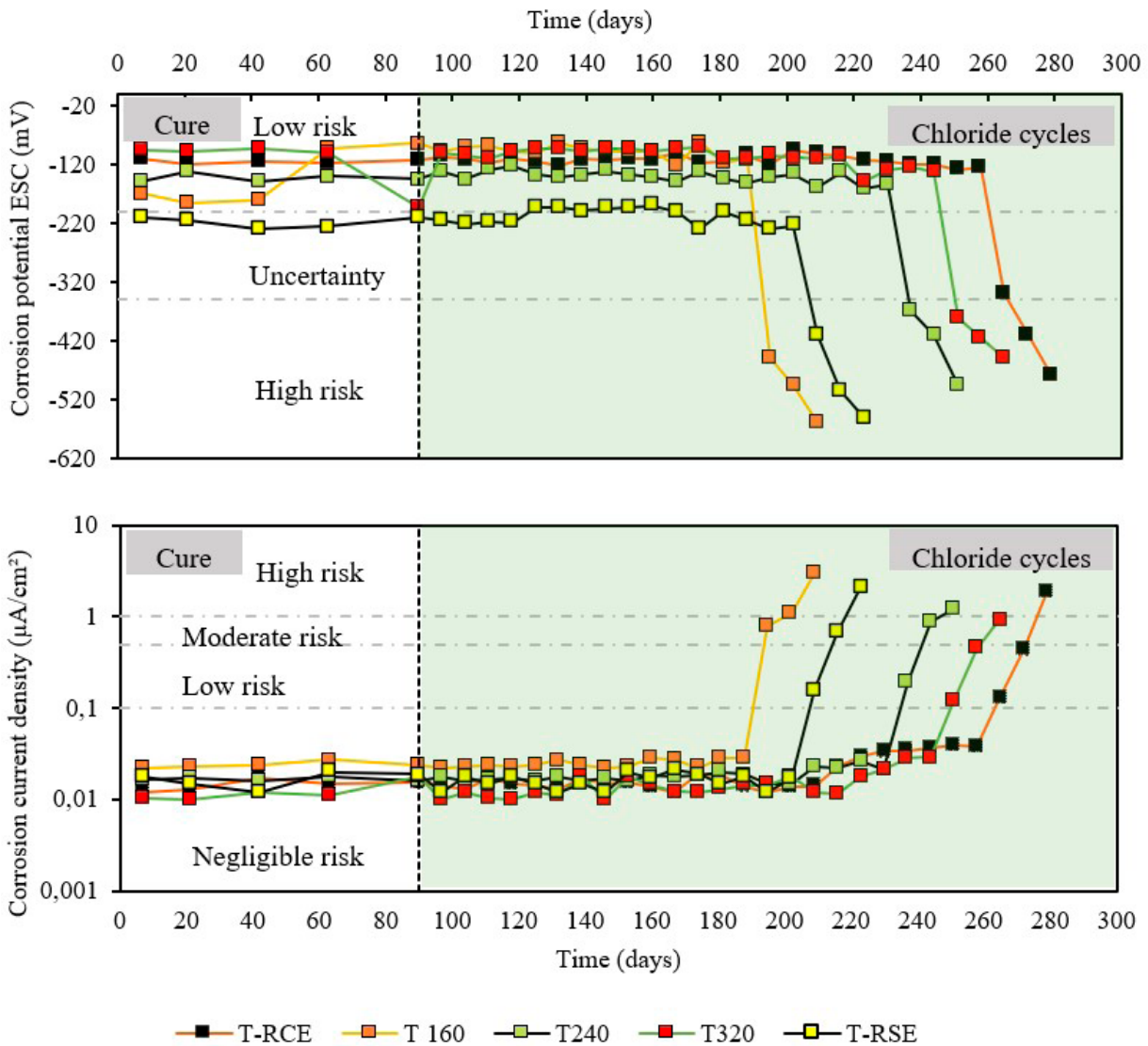


FIGURE 14. Electrochemical monitoring of the steel bars embedded in concrete (average results).

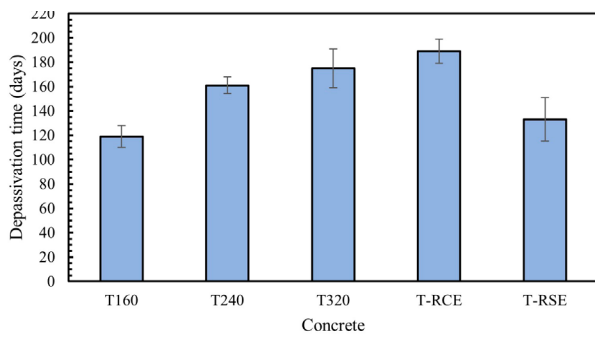


FIGURE 15. Depassivation time of bars embedded in concrete.

filler, exhibited greater water absorption coefficient than the T320 concrete, which was about 40% higher. Furthermore, particle packing, which determines the filling of voids, greatly affected the result of capillary absorption. The T-RCE concrete presented the best results in the water capillary absorption test, which presented a capillary absorption rate 56% lower than the reference mixture without packing.

The correlation between cement consumption and capillary absorption coefficient is better represented in Figure 13. Concrete with a high cement replacement rate, and consequently, lower content of this binder, yielded high absorption values. The Figure 13 also highlights the difference between concrete with packaging (T-RCE) and conventional reference concrete (T-RSE).

### 3.5. Electrochemical monitoring

Figure 14 shows the results of electrochemical monitoring of the steel bars embedded in concrete.

As expected, the steel bars embedded in T160 concrete, which had the lowest cement consumption, were the first to depassivate, requiring 119 days under wetting and drying cycles. T160 was closely followed by the reference concrete without aggregate packing (T-RSE) that showed a shift in the current density measurements after 133 days. Even with 57.19% less cement, T160 concrete presented a performance close to that of the conventional concrete (T-RSE). Figure 15 shows the reinforcement depassivation times for all concretes.

(44) studied concretes with ceramic residues (CR) and electrochemically monitored bars embedded in concrete with 10% and 30% of cement replacement by this residue, resulting in cement consumptions of 372.9 kg.m<sup>-3</sup> and 290 kg.m<sup>-3</sup>, respectively, and a reference concrete with cement consumption of 414.3 kg.m<sup>-3</sup>. The results of the electrochemical monitoring show that the passivation of the reference bars occurred in approximately 40 days, while that of the concrete with 10% RTM occurred in approximately 28 days and that of the concrete with 30% RTM occurred in 42 days. (68) monitored self-compacting concrete with an average cement consumption of 515 kg.m<sup>-3</sup>. Despite the high cement consumption, the bars depassivated after 50 days. Therefore, we can infer that the packaging of the aggregates applied in concretes T160, T240, and T320 compensated for the reduction in the cement content, thereby retarding the activation of rebars in these concretes.

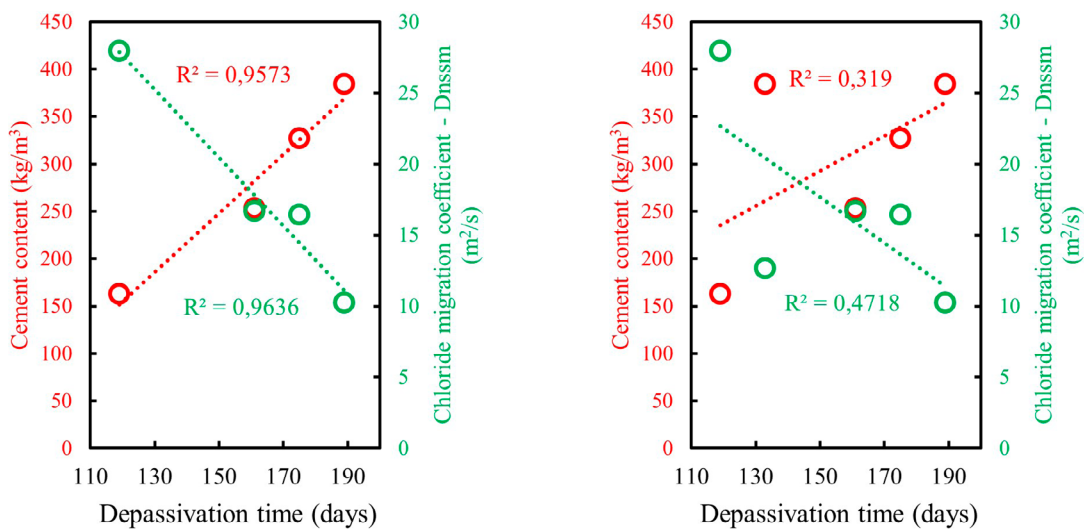


FIGURE 16. Correlations between cement content, depassivation time, and chloride migration coefficient, considering only packed concretes (a) and (b) all concretes.

The correlations shown in Figure 16 explain the effect of packaging on the initiation time of corrosion by chlorides. In the electrochemical monitoring, for the group of concretes with identical granular skeletons, cement content and chloride migration coefficient were strongly correlated (Figure 16 (a)). Since this also depends on the cement as the greater the clinker content, the greater is the aluminate content that can combine with the chlorides and fix them in the matrix, and in turn, longer is the depassivation time (69-71). Figure 16 (b) shows that there was no considerable correlation when comparing the concrete with packing with the reference concrete, even when the latter had a higher cement content. Thus, it was confirmed that the packing has a significant role in corrosion initiation retardation.

#### 4. CONCLUSION

From an analysis of the results presented in this paper, the following conclusions can be drawn:

- In general, when increasing limestone filler content, the compressive strength decreased compared with the reference concrete with packing (T-RCE). However, the concrete with cement consumption of 253.34 kg.m<sup>-3</sup> (T240) presented excellent results in the compressive strength test, with results quite close to those of the reference concrete with packing (T-RCE) and with superior performance than the other concretes containing limestone filler and the reference without packing.
- Concretes with limestone filler had higher binder efficiency than reference concrete, especially T-240, which presented a Bi about 30% lower than that of T-RCE, reinforcing the idea that there exists an ideal percentage of cement replacement by limestone filler to optimize concrete performance.
- The greater the replacement of cement by limestone filler, the greater was the chloride migration coefficient. However, this growth tendency tends to reduce when increasing the curing time from 28 to 90 days.
- The results of the T-240 concrete were very similar to those of concrete with cement consumption of 327.13 kg.m<sup>-3</sup> (T320). That is, even with a higher amount of filler, the results were similar to those of a mix with a lower mineral addition percentage in chloride migration and capillary absorption tests.
- In terms of capillary absorption by capillarity, the results of correlation with cement consumption confirmed that porosity is linked to cement

hydration products. However, the physical and chemical effects of the limestone filler, together with the packaging of the aggregates, contributed to concretes with cement replacement by lime filler present superior results than reference concrete without packing and with no cement replacement.

- Electrochemical monitoring showed that packing of the aggregates was essential to delay the initiation period of corrosion in concretes with a high limestone filler content.

In summary, the present work showed that applying packing concepts can make viable the use concretes with high levels of cement replacement by limestone filler and that there is an ideal level of cement replacement to maintain or increase the expected concrete performance. It is recommended that future work should analyze the critical content of chlorides in concrete with high levels of limestone filler.

#### Funding Sources

The authors would like to thank the Fundação de Apoio à Pesquisa do Estado Paraíba - FAPESQ for financing the research project.

#### Authorship contribution statement

**Robson Arruda dos Santos:** Conceptualization, Data curation, Formal analysis, Funding acquisition, Investigation, Methodology, Writing – original draft.

**Gibson Rocha Meira:** Formal analysis, Methodology, Writing – review & editing.

**Wilson Marques de Andrade Filho:** Conceptualization, Formal analysis, Investigation, Writing – original draft.

**Marina Cartaxo Braga Morais de Oliveira:** Conceptualization, Formal analysis, Investigation, Writing – original draft.

**Vitória Karoline Silva de Morais:** Conceptualization, Formal analysis, Investigation, Writing – original draft.

**José Matias Neto:** Formal analysis, Investigation, Writing – review & editing.

#### Declaration of competing interest

The authors of this article declare that they have no financial, professional or personal conflicts of interest that could have inappropriately influenced this work.

## REFERENCES

- Andrew R.M. 2019. Global CO<sub>2</sub> emissions from cement production, 1928–2018. *Earth System ScienceData*. 11(4):1675–1710. <https://doi.org/10.5194/essd-2019-152>.
- London. Global Construction 2030. 2020. Global Construction Perspectives; Oxford Economics. Retrieved from <https://www.oxfordeconomics.com/resource/future-of-construction/>.
- Yu R, Spiesz PR, Brouwers HJH. 2015. Development of ultra-high performance fibre reinforced concrete (UHPC): towards an efficient utilization of binders and fibres. *Constr. Build. Mater.* 79:273-282. <https://doi.org/10.1016/j.conbuildmat.2015.01.050>.
- Kanamarlapudi L, Jonalagadda KB, Jagarapu DCK, Eluru A. 2020. Different mineral admixtures in concrete: a review. *SN Appl. Sci.* 2:760. <https://doi.org/10.1007/s42452-020-2533-6>.
- Bessey GE. 1938. *Procd. Symp. Chem. Cements*. Stockholm.
- Soroka I, Setter N. 1977. The effect of fillers on strength of cement mortars. *Cem. Concr. Res.* 7(4):449-456. [https://doi.org/10.1016/0008-8846\(77\)90073-4](https://doi.org/10.1016/0008-8846(77)90073-4).
- Varhen C, Dilonardo I, Romano RCO, Pileggi RG, Figueiredo AD. 2016. Effect of the substitution of cement by limestone filler on the rheological behaviour and shrinkage of microconcretes. *Constr. Build. Mater.* 125:375-386. <https://doi.org/10.1016/j.conbuildmat.2016.08.062>.
- Liu SH, Gao ZY, Rao MJ. 2011. Study on ultra-high-performance concrete containing limestone powder. *Adv. Mater. Res. Trans Tech Publications Ltd*, 2011. 250-253:686-689. <https://www.scientific.net/AMR.250-253.686>.
- Cândido TG, Meira GR, Quattrone M, John M. 2022. Mechanical performance and chloride penetration resistance of concretes with low cement contents. *Rev. IBRACON Estrut. Mater.* 15(6):e15608. <https://doi.org/10.1590/S1983-41952022000600008>.
- Huang W, Kazemi-Kamyab H, Sun W, Scrivener K. 2017. Effect of cement substitution by limestone on the hydration and microstructural development of ultra-high performance concrete (UHPC). *Cem. Concr. Compos.* 77:86-101. <https://doi.org/10.1016/j.cemconcomp.2016.12.009>.
- Adu-Amankwah S, Zajac M, Stabler C, Lothenbach B, Black L. 2017. Influence of limestone on the hydration of ternary slag cements. *Cem. Concr. Res.* 100:96-109. <https://doi.org/10.1016/j.cemconres.2017.05.013>.
- Panesar DK, Zhang R. 2020. Performance comparison of cement replacing materials in concrete: Limestone fillers and supplementary cementing materials – A review. *Constr. Build. Mater.* 251:118866. <https://doi.org/10.1016/j.conbuildmat.2020.118866>.
- Cyr M, Lawrence P, Ringot E. 2006. Efficiency of mineral admixtures in mortars: Quantification of the physical and chemical effects of fine admixtures about compressive strength. *Cem. Concr. Res.* 36(2):264–277. <https://doi.org/10.1016/j.cemconres.2005.07.001>.
- Soroka I, Stern N. 1976. Calcareous fillers and the compressive strength of portland cement. *Cem. Concr. Res.* 6(3):367-376. [https://doi.org/10.1016/0008-8846\(76\)90099-5](https://doi.org/10.1016/0008-8846(76)90099-5).
- Luna F J, Fernández Á, Alonso MC. 2018). The influence of curing and aging on chloride transport through ternary blended cement concrete. *Mater. Construcc.* 68(332):e171. <https://doi.org/10.3989/mc.2018.11917>.
- Menéndez G, Bonavetti L, Irassar, EF. 2006. Ternary blended cement concrete. Part I: early age properties and mechanical strength. *Mater. Construcc.* 56(284):55–67. <https://doi.org/10.3989/mc.2006.v56.i284.18>.
- Bentz DP, Ardani A, Barrett T, Jones SZ, Lootens D, Peltz MA, Stutzman TSPE, Tanesi J, Weiss WJ. 2015. Multi-scale investigation of the performance of limestone in concrete. *Constr. Build. Mater.* 75:1-10. <https://doi.org/10.1016/j.conbuildmat.2014.10.042>.
- Berodier E, Scrivener K. 2014. Understanding the filler effect on the nucleation and growth of CSH. *J. Am. Ceram. Soc.* 97(12):3764–3773. <https://doi.org/10.1111/jace.13177>.
- Kakali G, Tsivilis S, Aggeli E, Bati M. 2000. Hydration products of C3A, C3S and Portland cement in the presence of CaCO<sub>3</sub>. *Cem. Concr. Res.* 30(7):1073-1077. [https://doi.org/10.1016/S0008-8846\(00\)00292-1](https://doi.org/10.1016/S0008-8846(00)00292-1).
- Menendez G, Bonavetti V, Irassar EF. 2003. Strength development of ternary blended cement with limestone filler and blast-furnace slag. *Cem. Concr. Compos.* 25(1):61–67. [https://doi.org/10.1016/S0958-9465\(01\)00056-7](https://doi.org/10.1016/S0958-9465(01)00056-7).
- Weerd, K, Haha MB, Saout G, Kjellsen KO, Justnes H, Lothenbach B. 2011. Hydration mechanisms of ternary Portland cements containing limestone powder and fly ash. *Cem. Concr. Res.* 41(3):279–291, <https://doi.org/10.1016/j.cemconres.2010.11.014>.
- Ghrici M, Kenai S, Said-Mansour M. 2007. Mechanical properties and durability of mortar and concrete containing natural pozzolana and limestone blended cements. *Cem. Concr. Compos.* 29(7):542-549. <https://doi.org/10.1016/j.cemconcomp.2007.04.009>.
- Sun J, Chen Z. 2018. Influences of limestone powder on the resistance of concretes to the chloride ion penetration and sulfate attack. *Powder Technol.* 338:725-733. <https://doi.org/10.1016/j.powtec.2018.07.041>.
- Steiner S, Proske T, Winnefeld F, Lothenbach B. 2022. Effect of limestone fillers on CO<sub>2</sub> and water vapour diffusion in carbonated concrete. *Cement.* 8:100027. <https://doi.org/10.1016/j.cement.2022.100027>.
- Mehta K. 1986. *Concrete: structure, properties, and materials*. Prentice Hall.
- Abushama WJ, Tamimi AK, Tabsh SW, El-Emam MM, Ibrahim A, Mohammed Ali TK. 2023. Influence of optimum particle packing on the macro and micro properties of sustainable concrete. *Sustainability.* 15(19):14331. <https://doi.org/10.3390/su151914331>.
- Oliveira IR. 2000. *Particle dispersion and packing: principles and applications in ceramic processing*. São Paulo: Making Editorial Art. 224.
- Santos RA, Meira GR, Bezerra WVDC, Braga FAV, Pontes DL. 2021. Use of numerical method for optimization of granulometric curves in eco-efficient concrete. *Matéria, Rio de Janeiro.* 26(4):e13115. <https://doi.org/10.1590/S1517-707620210004.1315>.
- Associação Brasileira de Normas Técnicas. 2018. ABNT NBR 16697: Cimento Portland – Requisitos. ABNT, Rio de Janeiro.
- Associação Brasileira de Normas Técnicas. 2017. NBR 16605: Cimento Portland e outros materiais em pó – determinação da massa específica. ABNT, Rio de Janeiro.
- Grazia MT, Sanchez LFM, Romano RCO, Pileggi RG. 2019. Investigation of the use of continuous particle packing models (PPMs). On the fresh and hardened properties of low-cement concrete (LCC). systems. *Construct. Build. Mater.* 195: 524–536. <https://doi.org/10.1016/j.conbuildmat.2018.11.051>.
- Associação Brasileira de Normas Técnicas. 2022. NBR 17054: Agregados – determinação da composição granulométrica. ABNT, Rio de Janeiro.
- Associação Brasileira de Normas Técnicas. 2021. ABNT NBR 16916 Agregado miúdo - Determinação da densidade e da absorção de água. ABNT, Rio de Janeiro.
- Associação Brasileira de Normas Técnicas. 2018. ABNT NBR 5739 Concreto - Ensaio de compressão de corpos de prova cilíndricos. ABNT, Rio de Janeiro.
- NT BUILD 492. 1999. Chloride migration coefficient from non-steady-state migration experiments.
- Associação Brasileira de Normas Técnicas. 2012. ABNT NBR 9779: Argamassa e concreto endurecidos — Determinação da absorção de água por capilaridade. ABNT, Rio de Janeiro.
- Associação Brasileira de Normas Técnicas. 2011. ABNT NBR 7222: Concreto e argamassa — Determinação da resistência à tração por compressão diametral de corpos de prova cilíndricos. ABNT, Rio de Janeiro.
- Page MM, Page CL, Ngala T, Anstice DJ. 2002. Ion chromatographic analysis of corrosion inhibitors in concrete.



- Constr. Build. Mater. 16(2):73-81. [https://doi.org/10.1016/S0950-0618\(02\)00017-X](https://doi.org/10.1016/S0950-0618(02)00017-X).
39. Vieira FMP. 2003. Contribuição ao estudo de corrosão de armaduras em concretos armados com adição de sílica ativa. Tese de doutorado em Engenharia, UFRGS, Porto Alegre – RS.
  40. Silva FG. 2006. Estudo de concretos de alto desempenho frente à ação de cloretos. Tese de Doutorado em Ciência e Engenharia dos Materiais, Escola Politécnica, Universidade de São Paulo, São Carlos – SP.
  41. Kishimoto I. 2010. Experimental study on the corrosion condition of steel bars in cracked reinforced concrete specimen. In: International Symposium on the Ageing Management & Maintenance of Nuclear Power Plants, 2010, Tokyo. Proceeding, Tokyo. 166-172.
  42. Angst UM, Vennesland Ø. 2009. Critical chloride content in reinforced concrete - State of the art. Concrete Repair, Rehabilitation and Retrofitting II. Taylor & Francis Group. 311- 317, London.
  43. Angst UM, Elsener B, Larsen CK, Vennesland Ø. 2011. Chloride induced reinforcement corrosion: electrochemical monitoring of initiation stage and chloride threshold values. Corros. Sci. 53(4):1451-1464. <https://doi.org/10.1016/j.corsci.2011.01.025>.
  44. Meira GR, Ferreira RR, Jerônimo L, Carneiro AMP. 2014. Comportamento de concreto armado com adição de resíduos de tijolo cerâmico moído frente à corrosão por cloretos. Ambiente Construído. 14(4):33-52. <https://doi.org/10.1590/S1678-86212014000400004>.
  45. Ferreira RR. 2015. Análise da indução da corrosão por cloretos em concretos armados com adição de resíduo de tijolo moído a partir de ensaios acelerados. Dissertação de Mestrado - Programa de Pós-Graduação em Engenharia Civil da Universidade Federal de Pernambuco (UFPE): Recife – PE.
  46. ASTM C876-09.2022. Standard test method for corrosion potentials of uncoated reinforcing steel in concrete.
  47. Fahim A, Ghods P, Isgor OB, Thomas MDA. 2018. A critical examination of corrosion rate measurement techniques applied to reinforcing steel in concrete. Mater. Corros. 69(12):1784-1799. <https://doi.org/10.1002/maco.201810263>.
  48. Alonso CA, Gulikers CJ, Polder R, Cigna OR, Vennesland MS, Raharinaivo A, Elsener B. 2004. Test methods for on-site corrosion rate measurement of steel reinforcement in concrete by means of the polarization resistance method. Mater. Struct. 37:623-643. <https://doi.org/10.1007/BF02483292>.
  49. Bederina M, Makhloufi Z, Bouziani T. 2011. Effect of limestone fillers the physic-mechanical properties of limestone concrete. Phys. Procedia. 21:28-34. <https://doi.org/10.1016/j.phpro.2011.10.005>.
  50. Wang D, Shi C, Farzadnia N, Shi Z, Jia H, Ou Z. 2018. A review on use of limestone powder in cement-based materials: Mechanism, hydration and microstructures. Constr. Build. Mater. 181:659-672. <https://doi.org/10.1016/j.conbuildmat.2018.06.075>.
  51. Damineli BL, Kemeid FM, Aguiar S, John M. 2010. Measuring the ecoefficiency of cement use. Cem. Concr. Compos. 32(8):555-562. <https://doi.org/10.1016/j.cemconcomp.2010.07.009>.
  52. Damineli BL. 2013. Concepts for the formulation of low binder consumption concrete: rheological control, packing, and particle dispersion. São Paulo: Polytechnic School of the University of São Paulo.
  53. Su N, Hsu KC, Chai HW. 2001. A simple mix design method for self-compacting concrete. Cem. Concr. Res. 31(12):1799-807. [https://doi.org/10.1016/S0008-8846\(01\)00566-X](https://doi.org/10.1016/S0008-8846(01)00566-X).
  54. Su N, Miao B. 2003. A new method for the mix design of medium strength flowing concrete with low cement content. Cem. Concr. Compos. 25(2):215-222. [https://doi.org/10.1016/S0958-9465\(02\)00013-6](https://doi.org/10.1016/S0958-9465(02)00013-6).
  55. Hüsken G, Brouwers HJH. 2008. A new mix design concept for earth-moist concrete: A theoretical and experimental study. Cem. Concr. Res. 38(10):1246-1259. <https://doi.org/10.1016/j.cemconres.2008.04.002>.
  56. Abd Elrahman M, Hillemeier B. 2014. Combined effect of fine fly ash and packing density on the properties of high-performance concrete: An experimental approach, Constr. Build. Mater. 58:225-233. <https://doi.org/10.1016/j.conbuildmat.2014.02.024>.
  57. Kanadasan J, Razak HA. 2014. Mix design for self-compacting palm oil clinker concrete based on particle packing, Materials & Design (1980-2015). 56:9-19. <https://doi.org/10.1016/j.matdes.2013.10.086>.
  58. Yu R, Van Onna DV, Spiesz P, Yu QL, Brouwers HJH. 2016. Development of ultra light weight fibre reinforced concrete applying expanded waste glass. J. Clean. Prod. 112(1):690-701. <https://doi.org/10.1016/j.jclepro.2015.07.082>.
  59. Sunayana S, Barai SV. 2017. Recycled aggregate concrete incorporating fly ash: Comparative study on particle packing and conventional method, Constr. Build. Mater. 156:376-86. <https://doi.org/10.1016/j.conbuildmat.2017.08.132>.
  60. Franco de Carvalho JM, Melo TV, Fontes WC, Batista JOS, Brigolini GJ, Peixoto RAF. 2019. More eco-efficient concrete: An approach on optimization in the production and use of waste-based supplementary cementing materials. Constr. Build. Mater. 206:397-409. <https://doi.org/10.1016/j.conbuildmat.2019.02.054>.
  61. Ashish DK, Verma SK. 2019. Determination of optimum mixture design method for self-compacting concrete: Validation of method with experimental results. Constr. Build. Mater. 217:664-678. <https://doi.org/10.1016/j.conbuildmat.2019.05.034>.
  62. Melo CVA, Gomes CC, Moraes KAM. 2019. A study of packing parameters that influence the fresh properties of self-compacting concrete. Cerâmica. 65(375):432-442. <https://doi.org/10.1590/0366-69132019653752667>.
  63. Lopes HMT, Peçanha ACC, Castro AL. 2020. Considerações sobre a eficiência de misturas de concreto de cimento Portland com base no conceito de empacotamento de partículas. Revista Materia. 25(1). <https://doi.org/10.1590/S1517-707620200001.0874>.
  64. Andrade, C. 1993. Calculation of chloride diffusion coefficients in concrete from ionic migration measurements. Cem. Concr. Res. 23(3):724-742. [https://doi.org/10.1016/0008-8846\(93\)90023-3](https://doi.org/10.1016/0008-8846(93)90023-3).
  65. Luna FJ, Fernández Á, Alonso MC. 2018. The influence of curing and aging on chloride transport through ternary blended cement concrete. Mater. Construcc. 68(332):e171. <https://doi.org/10.3989/mc.2018.11917>.
  66. Nilsson MH, Ngo Gjørø OE. 1998. High-performance repair materials for concrete structure in the port of Gothenburg, in concrete under severe conditions 2: Environment and loading. Proceedings of the Second International Conference on Concrete Under Severe Conditions. 2:1193-1198.
  67. Mehta K, Monteiro JM. 2014. Concrete: microstructure, properties, and materials. 4th ed. New York: McGraw-Hill Education.
  68. Jerônimo L, Meira GR, Filho LCS. 2018. Performance of self-compacting concrete with wastes from heavy ceramic industry against corrosion by chlorides. Constr. Build. Mater. 169:900-910. <https://doi.org/10.1016/j.conbuildmat.2018.03.034>.
  69. Ribeiro DV, Labrincha JA, Morelli MR. 2012. Effect of the addition of red mud on the corrosion parameters of reinforced concrete. Cem. Concr. Res. 42(1):124-133. <https://doi.org/10.1016/j.cemconres.2011.09.002>.
  70. Medeiros MHF, Rocha FC, Medeiros-Junior RA. 2017. Corrosion potential: influence of moisture, water-cement ratio, chloride content, and concrete cover. Rev. IBRACON Estrut. Mater. 10(4):864-885.
  71. Tian L, Dai S, Yao X, Zhu H, Wu Q, Liu Z, Cheng S. 2022. Effect of nucleation seeding and trisopropanolamine on the compressive strength, chloride binding capacity and microstructure of cement paste. J. Build. Eng. 52:104382. <https://doi.org/10.1016/j.job.2022.104382>.